

A Universal Formulation for Path-Parametric Planning and Control

Jon Arrizabalaga^{1,2}, Markus Ryll¹

October 8, 2024

Abstract

This work presents a unified framework for path-parametric planning and control. This formulation is universal as it standardizes the entire spectrum of path-parametric techniques – from traditional path following to more recent contouring or progress-maximizing Model Predictive Control and Reinforcement Learning – under a single framework. The ingredients underlying this universality are twofold: First, we present a compact and efficient technique capable of computing singularity-free, smooth and differentiable moving frames. Second, we derive a spatial path parameterization of the Cartesian coordinates applicable to any arbitrary curve without prior assumptions on its parametric speed or moving frame, and that perfectly interplays with the aforementioned path parameterization method. The combination of these two ingredients leads to a planning and control framework that brings together existing path-parametric techniques in literature. Aiming to unify all these approaches, we open source PACOR, a software library that implements the presented content, thereby providing a self-contained toolkit for the formulation of path-parametric planning and control methods.

PACOR, along with examples and documentation, is available at
<https://github.com/jonarriza96/PACOR>

1 Introduction

Path-parametric methods have gained popularity in the formulation of navigation algorithms, such as high-level planners [1, 2, 3], reinforcement learning (RL) policies [4, 5, 6] or low-level model predictive controllers (MPC) [7, 8, 9]. The fundamental concept behind these parametric methods is to either introduce the path parameter as an additional degree of freedom, enabling the system to regulate its progress along the path [10, 11], or to conduct a change of coordinates that project the *Euclidean states* to the *spatial states*, i.e., the progress along the path and the orthogonal distance to it [12, 13, 14]. These parametric formulations have proven successful for three primary reasons: firstly, they inherently capture the notion of advancement along the path, secondly they allow for embedding the path’s geometric features, such as the curvature and the torsion, into the system dynamics, and thirdly, spatial bounds manifest as convex constraints in the orthogonal terms of the spatial states.

Given the broad range of problems encompassing path-parametric approaches, existing methods remain detached from each other and are frequently presented as independent work. This has resulted in a disjointed body of literature, where these techniques are viewed as distinct methods. Consequently, the reader is left with a fragmented view of the path-parametric problem, making it difficult to understand the interplay between the different techniques. To close this gap, in this paper we show how all these approaches are interconnected by presenting a universal formulation for path-parametric planning and control.

To this end, the path-parametric problem is analyzed from three different yet interconnected perspectives (i-iii): First, in Section 2, we study the (i) *interplay of existing parametric techniques* and show how they can be unified under a single framework consisting of two ingredients: (ii) a *path-parameterization technique* and (iii) a *spatial representation of the system dynamics*. These are discussed in-depth across the subsequent Sections 3 and 4, respectively.

¹Munich Institute of Robotics and Machine Intelligence (MIRMI), Technical University of Munich (TUM)

²Robotics Institute (RI), Carnegie Mellon University (CMU)

2 Path-parametric planning and control

Before presenting a universal formulation for path-parametric planning and control, in this section, we formally introduce the problems we are addressing. Once we do so, we will show the conceptual connections between these methods and, finally, we will highlight how they can all be unified under a single framework.

2.1 An overview of path-parametric methods

Path-parametric methods are those that require from a reference path parameterized either by its arc-length or an arbitrary variable (we will further discuss this difference in Section 3). This variable is referred to as the *path-parameter* and it inherently captures the notion of progress along the path. The difference on how this path parameter is leveraged in the design of the planning and control algorithms is what distinguishes the different path-parametric methods. From a conceptual standpoint, these differences can be grouped according to two standards: the system states and the navigation criterion. The system states refer to the way the path parameter is introduced in the system dynamics, while the navigation criterion relates to how the path parameter is used in the planning and control algorithms.

Within the different system state representations, we distinguish three main categories: (i) *augmented states*, where the path parameter is introduced as an additional (virtual) degree of freedom in the system dynamics (ii) *projected states*, where the system dynamics are projected onto a coordinate system that is aligned with the reference path, and (iii) *transformed states*, where the system dynamics are transformed from the temporal domain to the spatial domain, causing them to evolve according to the path parameter instead of time.

The navigation criteria can also be grouped into three categories: (i) *progress or velocity profile regulation*, where the path-parameter’s speed is desired to follow a predefined speed profile, (ii) *time minimization*, where the aforementioned transformation from the temporal to the spatial domain is leveraged to convert the time minimization into a finite horizon problem, and (iii) *progress maximization*, where the path parameter is used to maximize the progress along the path.

Existing path-parametric methods in the literature result from combining one of the categories corresponding to the state representation with those within the navigation criteria. This is shown in Table 1, which provides an overview of the most relevant path-parametric methods in literature, alongside the system states and navigation criteria they use. The literature attached in the table is sorted by year of publication, and the specific method employed to implement the path-parametric representation: Control Law (CL), Optimization-based Planner (OP), Model Predictive Control (MPC) and Reinforcement Learning (RL). These wide spectrum demonstrates how path-parametric methods have evolved over time, becoming more sophisticated as the planning and control research fields have advanced.

2.2 A brief history: From Path Following to MPC and RL

The description of the complex shapes and motions encountered in the world is a fundamental pursuit in the sciences and engineering. While traditional Cartesian equations are adept at representing simple lines and circles, they often prove inadequate for capturing the intricacies of curves and surfaces observed in nature and human-made objects. This limitation necessitates the development of more versatile tools, and parametric equations emerge as a powerful solution. For example, parametric equations can be employed to express complex motions and paths, such as the trajectory of a projectile or the outline of a shape. For this reason, the concept of parameterizing a path by its arc length (or a proxy variable) has captivated the interest of humanity for centuries. Equally significant is the related idea of defining a curve by its curvature, a measure of “how much it bends.” The fascination with these methods of defining curves can be traced back to ancient Greece, where philosophers such as Aristotle and mathematicians like Archimedes explored these concepts. The advent of differential calculus in the 17th century introduced new tools and rekindled interest in this problem, attracting the attention of some of history’s greatest mathematicians, including Newton, Descartes, Leibniz, Euler, and Gauss. For a comprehensive account of the fascinating history of curve parameterization, please refer to [15].

In the realm of planning and control, the inception of path-parametric methods emerged in the 1980s, notably within the domain of robotic manipulators. Early endeavors identified the advantages of incorporating the path parameter in planning and control laws, such as rescaling infeasible trajectories [16] or computing end-effector motions for traversing a path in minimum

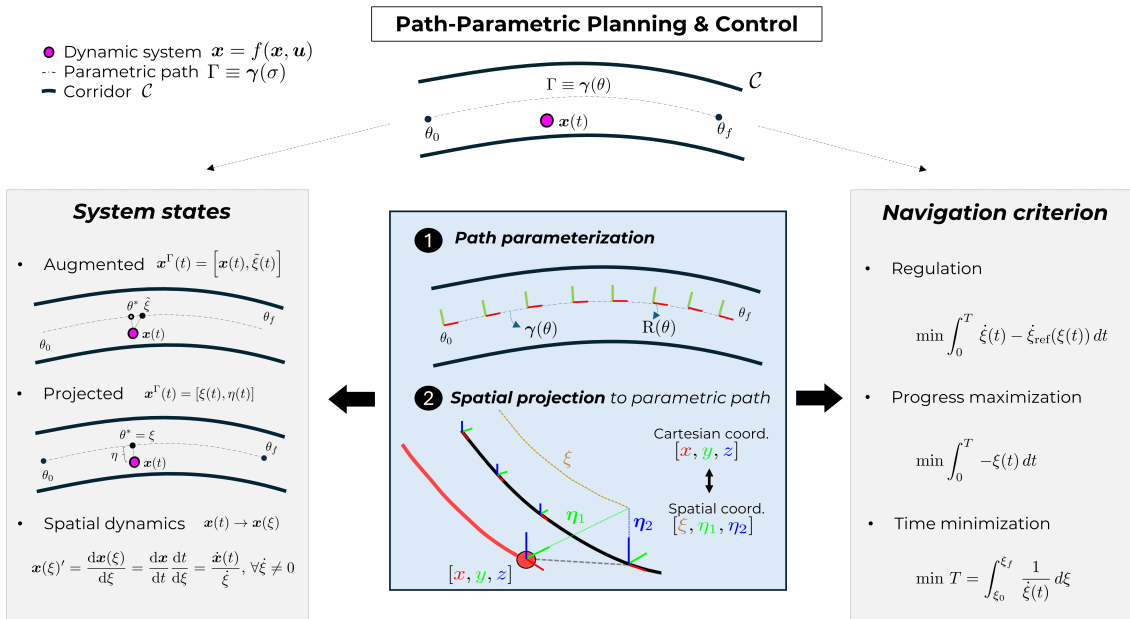


Figure 1: Path-parametric methods depend on a reference path that is parameterized by an auxiliary variable. These methods can be categorized based on the *system states* and *navigation criterion* (as indicated by the gray boxes). However, the literature on parametric methods is fragmented, with existing methods often presented as independent work. To bridge this gap, we demonstrate how these approaches are interconnected by introducing a universal formulation that involves two key components (highlighted in the blue box): (i) a path-parameterization technique to compute moving frames, and (ii) a spatial projection of the Cartesian system dynamics onto the parametric path, without any prior assumptions about the moving frame.

time [17, 18]. These works were the first leveraging the path parameter to transform the temporal dynamics into spatial dynamics, as explained in the previous subsection and depicted in Fig. 1. Soon thereafter, applications in the context of navigation for mobile robots appeared in [19, 20, 21], where the error to the path was decoupled into a tangent and an orthogonal component. This decoupling allowed for the design of control laws that regulated the progress along the path, while ensuring the robot would always converge to it. These findings sowed the seed for upcoming more sophisticated formulations, such as the works under the spatial projections category (column 7 in Table 1 and Fig. 1). The subsequent years served for establishing the theoretical foundations and getting a better understanding of these formulations [22, 23], resulting in the articulation of *path-following* as a distinct and superior alternative to path-tracking [24, 25, 26, 11].

These findings paved the ground for a new era, where the applicability of path-parametric methods shifted from closed-form solutions obtained with classical control to optimization-based formulations. This transition is constituted by two separate lines of work which laid the foundations for multiple applications and extensions, ultimately becoming the top contributors for the attention that path-parametric methods receive today. On the one hand, in the seminal work [12], it was shown that traversing a path in minimum time with a robotic manipulator – originally tackled in [17, 18] – can be formulated as a convex optimization problem. On the other hand, [27, 10] shed some light on the appealing attributes that result from embedding the tangent and orthogonal error components – originally introduced in [19, 20, 21] – into an optimization problem that is solved in a receding horizon (or MPC) fashion. For the first time, this provided the capacity to deviate from the path, allowing the user to trade-off between traversability and tracking accuracy. Despite the technical differences between [10] and [27], this line of work is commonly referred to as Contouring Control¹.

These two lines of works laid the foundations that, combined with advances in numerical solvers and an increases in computational power, led to a boom in the applicability of path-parametric methods, especially in the context of receding horizon optimization-based control algorithms (MPC). Most of the successful applications of path-parametric methods in real-world systems can be found in this family of works. Additionally, the advent of Reinforcement Learning (RL) brought yet another

¹Due to its usage within receding horizon optimization, it is commonly denoted as Model Predictive Contouring Control (MPCC)

Table 1: Path-parametric approaches sorted by the year, system applicability, methodology, capacity to account for deviations from the path, system state representation and navigation criterion. The methods are "Control Law" (CL), "Optimization-based Planner" (OP), "Model Predictive Control" (MPC), "Reinforcement Learning" (RL), and for those that do not fit into any of the previous, "Other" (OT).

Ref.	Year	System	Method	Dev.	System states			Navigation criterion		
					Augm.	Proj.	Transf.	Reg.	Time	Progr.
[16]	1984	Rob. Mani.	OT	✗			•	•		
[17]	1985	Rob. Mani.	OP	✗			•		•	
[18]	1987	Rob. Mani.	OT	✗			•		•	
[19]	1988	UGV	CL	✗	•			•		
[20]	1990	UGV	CL	✗	•			•		
[21]	1991	UGV	CL	✗	•			•		
[22]	1995	Any ¹	CL	✗	•			•		
[23]	2004	Any	CL	✗	•			•		
[24]	2004	Ship	CL	✗	•			•		
[25]	2005	Any	CL	✗	•			•		
[26]	2007	Underactuated	CL	✗	•			•		
[12]	2009	Rob. Mani.	OP	✗			•		•	
[27]	2009	Any	MPC	✓	•			•		
[10]	2010	Any	MPC	✗		•				•
[28]	2011	Car	MPC	✓			•		•	
[29]	2012	Car	MPC	✓			•		•	
[30]	2013	Rob. Mani.	MPC	✗	•			•		
[31]	2013	Car	MPC	✓			•			
[32]	2013	Crane	MPC	✗	•			•		
[7]	2015	Car	MPC	✓	•					•
[11]	2015	Any	MPC	✓	•			•		
[13]	2016	Rob. manip.	MPC	✓			•	•		
[1]	2016	Rob. manip.	OP	✓			•		•	
[33]	2017	Quadrotor	CL	✗		•		•		
[2]	2017	Quadrotor	OP	✓			•		•	
[34]	2019	Car	MPC	✓	•					•
[35]	2020	Car	MPC	✓		•		•		
[36]	2021	Car	MPC	✓		•		•		
[37]	2021	Quadrotor	MPC	✓	•					•
[9]	2022	Quadrotor	MPC	✓		•		•		
[38]	2022	Quadrotor	MPC	✗	•					•
[14]	2022	Particle	MPC	✓		•				•
[5]	2022	Quadrotor	RL	✓	•					•
[39]	2023	Particle	CL	✗	•			•		
[3]	2023	Car, Quadrotor	OP	✓			•		•	
[40]	2023	Car	MPC	✓		•		•		
[41]	2023	Quadrotor	OP	✓			•		•	
[6]	2023	Quadrotor	RL	✓	•					•
[8]	2024	Rob. manip.	MPC	✓		•		•		
[42]	2024	Quadrotor	MPC	✓	•					•

¹ Any system that is feedback linearizable

use to the path-parametric problem, where the notion of progress and other geometric features inherent to the path-parametric methods became very appealing for the design of the reward function. Compared to the previous solutions, most of these methods allowed deviations from the path by relying on collision-free tunnels, tubes or corridors. This led to a paradigm shift, where instead of committing to a given path, any trajectory within the admissible space is valid, a very attractive feature for case studies with constrained task spaces. As a consequence, the resulting literature broadened across a wide range of applications, such as autonomous driving [28, 29, 31, 7, 34, 35, 40], autonomous agile flight [2, 37, 9, 38, 41, 6], robotic manipulators [1, 13] or more exotic cases like cranes [32].

From the overview in this subsection it is apparent that path-parametric methods have progressed significantly, spanning across various applications and methodologies. To illustrate this clearly, we have categorized all the aforementioned works in Table 1. From this table, we characterize path-parametric methods according to three observations: First, they are a combination of the

system state representation and the navigation criteria explained in the previous subsection, and thus, can be grouped accordingly. Second, the rise of new gradient-based techniques within planning and control, such as optimization and learning, have driven the evolution of path-parametric methods. Third, these methods have become more sophisticated over time, allowing for deviations from the path, and thereby, increasing the applicability to a wider range of problems.

2.3 A universal formulation for all path-parametric methods

As discussed earlier, path-parametric methods have evolved to meet the diverse needs of the planning and control communities. This evolution has significantly expanded their application across various domains, resulting in a wide array of real-world implementations. However, this has resulted in a more disjointed literature, with each method often presented in isolation. This fragmented approach has created a scattered body of knowledge where these techniques are perceived as distinct entities, making it challenging for readers to grasp their interconnectedness and broader implications.

To address this gap, this paper aims to demonstrate the unified nature of path-parametric planning and control methods. We show how these approaches are inherently linked by introducing a universal formulation. Central to this formulation are two fundamental components that underpin all existing works in the literature. These components are: (i) the method of path parameterization, which defines how the desired geometric reference is articulated, and (ii) the representation of system dynamics relative to this path parameterization, crucial for understanding how the system behaves along the specified path.

Currently, the literature lacks a generic treatment of these components, contributing to its fragmented nature. By establishing a generalized approach that transcends specific methodologies, we aim to unify path-parametric techniques into a single framework that encompasses everything from traditional path following control laws to more advanced optimization and learning-based methods. In the remainder of the manuscript, we delve into the details necessary to formulate these two foundational ingredients, while ensuring that they meet the demands outlined earlier. Through this unified framework, we seek to not only consolidate existing knowledge but also facilitate the future development and application of path-parametric methods across diverse fields.

Notation

We will use $(\dot{\cdot}) = \frac{d(\cdot)}{dt}$ for time derivatives and $(\cdot)' = \frac{d(\cdot)}{d\theta}$ for differentiating over path parameter θ .

3 Path parameterizing the reference path

In this section, we focus on the first ingredient of the universal framework, namely the method used to transcribe the reference path into a parametric function. We do this in three separate steps: First, we formally define the geometric reference as a parametric function with a moving frame attached to it. Second, we refer to the problem of computing this frame, by considering the existing options, and third, we present an efficient, simple and compact algorithm for this task.

3.1 Assigning a path parameter to the reference path

Existing autonomous navigation systems define the reference path either as a set of waypoints [43] or as a parametric function determined by a higher-level planner [44, 45]. In the first scenario, where the reference is characterized by a collection of waypoints $\mathbf{wp} = [\mathbf{wp}_1, \mathbf{wp}_2, \dots, \mathbf{wp}_n] \in \mathbb{R}^{3 \times n}$, the path parameterization is done by interpolating these waypoints with a smooth curve, as in [46]. In the second scenario, this interpolation step is unnecessary because the higher-level planner directly provides a predetermined parametric function formulation, such as B-splines. In either case, the reference path is ultimately expressed as a smooth parametric function $\gamma : \mathbb{R} \mapsto \mathbb{R}^3$, dependent on the *path parameter* θ . This implies that the *arc-length* of the reference is given by

$$l(\theta) = \int_{\theta_0}^{\theta} \|\gamma'(\theta)\| d\theta, \quad (1)$$

highlighting a distinction often misunderstood in literature, namely, that the arc-length $l(\theta)$ is distinct from the path parameter θ . To better understand this concept, we define the term inside the integral as the *parametric speed*:

$$\sigma(\theta) = \|\gamma'(\theta)\|. \quad (2)$$

Intuitively, the parametric speed captures the variation of the path parameter θ with respect to the arc-length $l(\theta)$. Hence, only when $\sigma = 1$ do the arc-length and the path parameter coincide, resulting in a reference path parameterized by its arc-length².

3.2 Assigning a moving frame to the reference path

The ability to decouple the system dynamics into tangential and orthogonal components relative to the reference path is fundamental to path-parametric formulations. This decoupling facilitates the design of algorithms that guide the system along the path while limiting deviations from it. To achieve this, it is necessary to define a local frame that evolves with the path. As such, we augment the position function $\gamma(\theta)$ by attaching a moving frame whose rotation matrix is given by another parametric function $\mathbf{R} : \mathbb{R} \mapsto \mathbb{R}^{3 \times 3}$ also parameterized by θ . Combining it with the position function $\gamma(\theta)$ introduced in the previous subsection formally defines the *geometric reference* as:

$$\Gamma = \{\theta \in [\theta_0, \theta_f] \subseteq \mathbb{R} \mapsto \gamma(\theta) \in \mathbb{R}^3, \mathbf{R}(\theta) \in \mathbb{R}^{3 \times 3}\}. \quad (3)$$

We refer to the moving frame $\mathbf{R}(\theta) = [\mathbf{e}_1(\theta), \mathbf{e}_2(\theta), \mathbf{e}_3(\theta)]$ as the *path-frame* $(\cdot)^\Gamma$ and is assumed to be *adapted*, i.e., the first component of the frame coincides with the path's tangent $\mathbf{e}_1(\theta) = \frac{\gamma'(\theta)}{\|\gamma'(\theta)\|} = \frac{\gamma'(\theta)}{\sigma(\theta)}$. The change of this frame with respect to the path parameter is determined by the angular velocity $\boldsymbol{\omega}(\theta) = [\omega_1(\theta), \omega_2(\theta), \omega_3(\theta)]$, which can also be represented in the path-frame as $\boldsymbol{\omega}^\Gamma(\theta) = [\omega_1^\Gamma(\theta), \omega_2^\Gamma(\theta), \omega_3^\Gamma(\theta)]$:

$$\boldsymbol{\omega}(\theta) = \boldsymbol{\omega}^\Gamma(\theta) \mathbf{R}^\top(\theta) = \omega_1^\Gamma(\theta) \mathbf{e}_1(\theta) + \omega_2^\Gamma(\theta) \mathbf{e}_2(\theta) + \omega_3^\Gamma(\theta) \mathbf{e}_3(\theta). \quad (4)$$

In either case, the motion of the moving frame $\mathbf{R}(\theta)$ is given by

$$\mathbf{R}'(\theta) = \overbrace{\begin{bmatrix} 0 & -\omega_3(\theta) & \omega_2(\theta) \\ \omega_3(\theta) & 0 & -\omega_1(\theta) \\ -\omega_2(\theta) & \omega_1(\theta) & 0 \end{bmatrix}}^{\Omega(\theta)} \mathbf{R}(\theta) \equiv \mathbf{R}(\theta) \overbrace{\begin{bmatrix} 0 & -\omega_3^\Gamma(\theta) & \omega_2^\Gamma(\theta) \\ \omega_3^\Gamma(\theta) & 0 & -\omega_1^\Gamma(\theta) \\ -\omega_2^\Gamma(\theta) & \omega_1^\Gamma(\theta) & 0 \end{bmatrix}}^{\Omega^\Gamma(\theta)} \quad (5)$$

where $\Omega(\theta)$ and $\Omega^\Gamma(\theta)$ are the skew symmetric matrices associated to the angular velocity vectors in world-frame $\boldsymbol{\omega}(\theta)$ and path-frame $\boldsymbol{\omega}^\Gamma(\theta)$, respectively³. From (5), it follows that the components of the angular velocity in the moving frame are given by

$$\omega_1^\Gamma(\theta) = \mathbf{e}_2'(\theta) \mathbf{e}_3(\theta), \quad \omega_2^\Gamma(\theta) = \mathbf{e}_3'(\theta) \mathbf{e}_1(\theta), \quad \omega_3^\Gamma(\theta) = \mathbf{e}_1'(\theta) \mathbf{e}_2(\theta). \quad (6)$$

As will become apparent in the upcoming section, the angular velocities of the moving frames correspond to the *curvature* κ and *torsion* τ of the path, and their computation is highly dependant on the choice of the moving frame. Subsequently, we will delve into the different options for describing the moving frame, and ultimately present an efficient, simple and compact algorithm for their computation.

3.3 Choosing a moving frame

The path-frame associated to the geometric reference Γ in (3) plays a crucial role in the formulation of path-parametric methods, since it allows for decoupling the system dynamics into components tangential and orthogonal to the path. This raises the need for a technique to augment the position function $\gamma(\theta)$ into a moving frame $\mathbf{R}(\theta)$, i.e., a method that solely requires a parametric position reference to compute a frame that evolves with it.

This is a well-studied problem with multiple solutions available in the existing literature, each differing based on the choice of the underlying frame. The most common options are the Frenet Serret Frame (FSF) [48, 49], the Euler Rodrigues Frame (ERF) [50, 51] and the Parallel Transport Frame (PTF) [52, 53, 54]. From a computation perspective, the first two frames are analytical, as they are given in closed form by local derivative information, while the latter requires from global information, and thus, its computation relies on a numerical routine.

The most common choice in the literature is the FSF due to its analytical simplicity. However, it is undefined when the reference path is a straight line (i.e., when the curvature vanishes) and introduces an unnecessary twist over its first component, causing undesired nonlinearities when projecting system dynamics to the path frame or representing the collision-free space around the

²For further details on how to path parameterize the reference path by its arc-length, please refer to [46]

³For a detailed proof of the equivalence in eq. (5), please see Theorem 1 in [47]

path. Within analytical frames, an alternative is the ERF, which remains defined even if the reference path is straight. However, the ERF cannot be guaranteed to be twist-free and relies on a Pythagorean Hodograph curve, whose computation is complex and may require numerical routines. Consequently, the most common alternative to the FSF is the PTF, which is both singularity-free and twist-free but requires numerical computation.

Existing methods to compute PTFs are discrete [54], and thus do not allow for the computation of higher derivatives. Additionally, they focus exclusively on the computation of the rotation matrix and neglect its angular velocity. However, as explained in Section 2.2, current path-parametric methods heavily rely on learning and optimization algorithms, which require first and second order derivatives. To address this, in this manuscript we present an efficient, simple, and compact method based on PTFs that computes the components and angular velocity of a singularity-free and twist-free path frame, while also accounting for the computation of the respective derivatives. Aiming to make this manuscript self-contained, before presenting this algorithm, we also provide an overview of the alternative methods.

Table 2: A comparison of methods for computing moving frames: Frenet Serret Frame (FSF), Parallel Transport Frame (PTF), Euler Rodrigues Frame (ERF).

Frame	Singularity-free	Twist-free
Frenet Serret	✗	✗
Euler Rodrigues	✓	✗
Parallel Transport	✓	✓

Frenet Serret Frame (FSF)

The Frenet Serret frame is defined by imposing the second component to be the normalized derivative of the tangent, and the third component orthogonal to the first and second.

$$\mathbf{e}_2(\theta) = \frac{\mathbf{e}'_1(\theta)}{\|\mathbf{e}'_1(\theta)\|}, \quad \mathbf{e}_3(\theta) = \mathbf{e}_1(\theta) \times \mathbf{e}_2(\theta). \quad (7a)$$

Combining these with the tangent component \mathbf{e}_1 , we can explicitly define the FSF by the path function $\gamma(\theta)$ and its derivatives:

$$\mathbf{e}_1(\theta) = \frac{\gamma'(\theta)}{\|\gamma'(\theta)\|}, \quad \mathbf{e}_2(\theta) = \frac{\gamma'(\theta) \times (\gamma''(\theta) \times \gamma'(\theta))}{\|\gamma'(\theta)\| \cdot \|\gamma''(\theta) \times \gamma'(\theta)\|}, \quad \mathbf{e}_3(\theta) = \frac{\gamma'(\theta) \times \gamma''(\theta)}{\|\gamma'(\theta) \times \gamma''(\theta)\|}. \quad (7b)$$

Given that the frame is exclusively dependant on the derivatives at the evaluating point, FSF is a *local frame*, i.e., the frame can be evaluated by only relying on local derivative information. Notice that the second component is not defined when γ' and γ'' are parallel. To understand the meaning of this, we need to calculate the angular velocity of the frame ω_{FSF} . To compute it, we combine the eqs. in (4) with (7), resulting in

$$\omega_{\text{FSF},1}^\Gamma = \mathbf{e}'_2(\theta) \mathbf{e}_3(\theta) = \sigma(\theta) \tau(\theta), \quad (8a)$$

$$\omega_{\text{FSF},2}^\Gamma = \mathbf{e}'_3(\theta) \mathbf{e}_1(\theta) = 0, \quad (8b)$$

$$\omega_{\text{FSF},3}^\Gamma = \mathbf{e}'_1(\theta) \mathbf{e}_2(\theta) = \sigma(\theta) \kappa(\theta). \quad (8c)$$

where the first and third components relate to the *torsion* $\tau(\theta)$ and *curvature* $\kappa(\theta)$, respectively. Intuitively, these express how the curve twists (corridor) over the first component or bends over the third component (road). Mathematically, they are given by:

$$\tau(\theta) = \frac{\omega_{\text{FSF},1}^\Gamma(\theta)}{\sigma(\theta)} = \frac{\|(\gamma'(\theta) \times \gamma''(\theta)) \cdot \gamma'''(\theta)\|}{\|\gamma'(\theta) \times \gamma''(\theta)\|^2}, \quad \kappa(\theta) = \frac{\omega_{\text{FSF},3}^\Gamma(\theta)}{\sigma(\theta)} = \frac{\|\gamma'(\theta) \times \gamma''(\theta)\|}{\|\gamma'(\theta)\|^3}. \quad (8d)$$

Notice that the parametric speed $\sigma(\theta)$ is decoupled from the curvature $\kappa(\theta)$ and torsion $\tau(\theta)$, proving that they are agnostic to the underlying path-parameterization. Putting all together, we can compute the angular velocity of the frame as:

$$\omega_{\text{FSF}}(\theta) = \omega_{\text{FSF},1}^\Gamma(\theta) \mathbf{e}_1(\theta) + \omega_{\text{FSF},3}^\Gamma(\theta) \mathbf{e}_3 = \sigma(\theta) (\tau(\theta) \mathbf{e}_1(\theta) + \kappa(\theta) \mathbf{e}_2(\theta)). \quad (8e)$$

From (8), it is apparent that the FSF is characterized by $\omega_{\text{FSF},2}^\Gamma = 0$ (second component always pointing to the center of the curve). This implies that (i) it has singularities when curvature

vanishes and (ii) the frame flips when the path transitions from left to right turn. Additionally, it contains a twist along the tangent component, which results in a non-realistic motion of the frame. Therefore we look into alternative moving frames.

Euler Rodrigues Frame

The ERF presents a potential solution to the limitations of the FSF. It is fully defined, i.e., has no singularities even when the reference path is straight, and it is a local frame, implying that it can be calculated by exclusively relying on local derivative information. However, the ERF is constructed upon a Pythagorean Hodograph (PH) curve, a subset of polynomials characterized by the property that the parametric speed $\sigma(\theta)$ is a polynomial on the path parameter θ . Imposing this condition, results in a family of polynomials whose geometric features, such as the arclength, curvature, torsion, etc. can be computed in closed form, by exclusively relying on rational functions. Another benefit of these polynomials is that they inherit an adapted frame, the ERF, which is fully defined and, for a given PH curve, their computation is straightforward.

However, converting a given reference path $\gamma(\theta)$ into a PH curve is not a trivial task, and may require numerical routines. Moreover, guaranteeing differentiability and continuity of the ERF and its angular velocity further increases the complexity of the conversion. Besides that, the algebra and calculus involved in the computation of PH curves and their corresponding ERFs are highly involved, introducing an additional layer of complexity and making them less prone to be reproduced by practitioners within the planning and control communities. Given the amount of detail required to derive and compute these curves and frames, they will be omitted in this manuscript. For further information on PH curves and ERFs, see [55] and [50], respectively. A more applied perspective with navigation applications leveraging PH curves and ERFs can be found in [14, 3, 39]. Lastly, if you are interested in the construction of PH curves and ERFs for path-parametric planning and control algorithms, a real-time and two times differentiable algorithm is given in our accompanying manuscript [56].

Parallel Transport Frame

The PTF offers a solution to the shortcomings of the FSF, as well as the ERF. Not only it is fully defined and can be twist-free, but its implementation is also very simple, making it lightweight, efficient and easy to reproduce. These reasons make the PTFs the most suitable choice for path-parametric planning and control algorithms. Their construction is spread out across the literature [53, 54, 41], but none of them addresses the computation of the moving frame's differentiability and angular velocity. Therefore, in this subsection we present an efficient, simple and compact algorithm that given a parametric curve $\gamma(\theta)$, finds the associated PTF and angular velocity $R_{\text{PTF}}(\theta)$, $\omega_{\text{PTF}}(\theta)$, while also accounting for the respective derivatives. Before presenting this algorithm, we provide an overview of the PTF.

The PTF originates from the seminal work *There is more than one way to frame a curve* [52], which raises the realization that the second \mathbf{e}_2 and third \mathbf{e}_3 components of the moving frame can be chosen freely, as long as they remain in the orthogonal plane and form an orthonormal frame with the remaining tangent component \mathbf{e}_1 . This allows for choosing the second and third components to form a parallel vector field that only rotates by the necessary amount, so that it is always perpendicular to the tangent component. This is equivalent to imposing the derivative of the second and third components to point in the direction of the tangential unit vector:

$$\mathbf{e}'_2(\theta) = k_1(\theta)\mathbf{e}_1(\theta), \quad \mathbf{e}'_3(\theta) = k_2(\theta)\mathbf{e}_1(\theta). \quad (9a)$$

To compute the auxiliary variables k_1 and k_2 , we combine (9a) with the orthonormality conditions

$$0 = 1 - \mathbf{e}_2^\top(\theta)\mathbf{e}_2(\theta), \quad 0 = 1 - \mathbf{e}_3^\top(\theta)\mathbf{e}_3(\theta) \quad (9b)$$

$$0 = \mathbf{e}_1^\top(\theta)\mathbf{e}_2(\theta), \quad 0 = \mathbf{e}_1^\top(\theta)\mathbf{e}_3(\theta). \quad (9c)$$

Differentiating (9c) with path parameter θ , combining it with (9a) and multiplying with $\mathbf{e}_1(\theta)$, we get

$$k_1(\theta) = -\mathbf{e}'_1(\theta)^\top \mathbf{e}_2(\theta), \quad k_2(\theta) = -\mathbf{e}'_1(\theta)^\top \mathbf{e}_3(\theta),$$

which ultimately leads to

$$\mathbf{e}'_2(\theta) = \left(-\mathbf{e}'_1(\theta)^\top \mathbf{e}_2(\theta)\right) \mathbf{e}_1(\theta), \quad \mathbf{e}'_3(\theta) = \left(-\mathbf{e}'_1(\theta)^\top \mathbf{e}_3(\theta)\right) \mathbf{e}_1(\theta). \quad (10)$$

Eqs. (10) provide the key insight required to compute the angular velocity of the PTF. By merging them with the definitions of the angular velocity for a generic moving frame in (6), we get

$$\omega_{\text{PTF},1}^{\Gamma}(\theta) = \mathbf{e}'_2(\theta)\mathbf{e}_3(\theta) = \left(-\mathbf{e}'_1(\theta)^{\top}\mathbf{e}_2(\theta)\mathbf{e}_1(\theta)\right)\mathbf{e}_3(\theta) = 0, \quad (11a)$$

$$\omega_{\text{PTF},2}^{\Gamma}(\theta) = \mathbf{e}'_3(\theta)\mathbf{e}_1(\theta) = \left(-\mathbf{e}'_1(\theta)^{\top}\mathbf{e}_3(\theta)\mathbf{e}_1(\theta)\right)\mathbf{e}_1(\theta) = -\mathbf{e}'_1(\theta)^{\top}\mathbf{e}_3(\theta), \quad (11b)$$

$$\omega_{\text{PTF},3}^{\Gamma}(\theta) = \mathbf{e}'_1(\theta)\mathbf{e}_2(\theta). \quad (11c)$$

where $(\cdot)^{\Gamma}$ indicates that the angular velocity is expressed in the path-frame Γ . When translated to the world-frame as defined in (4), it becomes

$$\boldsymbol{\omega}_{\text{PTF}}(\theta) = \boldsymbol{\omega}_{\text{PTF}}^{\Gamma}(\theta)\mathbf{R}_{\text{RMF}}^{\top}(\theta) = \omega_{\text{PTF},2}^{\Gamma}(\theta)\mathbf{e}_2(\theta) + \omega_{\text{PTF},3}^{\Gamma}(\theta)\mathbf{e}_3(\theta). \quad (11d)$$

From eqs. (11), there are two key insights to be drawn. First, in contrast to the FSF in (8), the angular velocity of the PTF does not have a component along the tangent \mathbf{e}_1 , i.e., $\omega_{\text{PTF},1}^{\Gamma} = 0$, and thus, the PTF is twist-free. Second, the angular velocity $\boldsymbol{\omega}_{\text{PTF}}(\theta)$ is exclusively dependant on the second and third components of the moving frame $\mathbf{R}_{\text{PTF}}(\theta)$ and the derivative of its tangent $\mathbf{e}'_1(\theta)$. Thus, if the initial frame is given $\mathbf{R}_{\text{PTF}}(\theta_0) = [\mathbf{e}_1(\theta_0), \mathbf{e}_2(\theta_0), \mathbf{e}_3(\theta_0)]$, we can compute the PTF at any point along the curve by forward integrating it as

$$\mathbf{R}_{\text{PTF}}(\theta_{i+1}) = e^{\Omega_{\text{PTF}}(\theta_i)\Delta\theta_i}\mathbf{R}_{\text{PTF}}(\theta_i), \quad (12)$$

where $\Delta\theta_i = \theta_{i+1} - \theta_i$ and $\Omega_{\text{PTF}}(\theta_i)$ refers to the skew symmetric matrix associated with the angular velocity $\boldsymbol{\omega}_{\text{PTF}}$, as defined in (5). Notice that $\mathbf{e}'_1(\theta)$ drives the integration forward, and thus, the reference path $\gamma(\theta)$ needs to be at least C^2 . Additionally, conducting the integration within $\text{SO}(3)$, ensures that the frame remains orthonormal, in contrast to other standard methods, such as Euler or Runge-Kutta [57]. Algorithm 1 summarizes the steps required to compute the PTF and its angular velocity.

Algorithm 1 *Parallel Transport Frame Integration (PTFI):*

Input: $\theta_0, \dots, \theta_N, \mathbf{R}_{\text{PTF}}(\theta_0), \mathbf{e}_1(\theta_0, \dots, \theta_N)$

Output: $\mathbf{R}_{\text{PTF}}(\theta_0, \dots, \theta_N), \boldsymbol{\omega}_{\text{PTF}}(\theta_0, \dots, \theta_N)$

```

1: function PTFI( $\theta_0, \dots, \theta_N, \mathbf{R}_{\text{PTF}}(\theta_0), \mathbf{e}'_1(\theta_0, \dots, \theta_N)$ )
2:   for  $i \in \{0, \dots, N-1\}$  do
3:      $\boldsymbol{\omega}_{\text{PTF}}(\theta_i) \leftarrow \text{ANGULARVEL}(\mathbf{e}'_1(\theta_i), \mathbf{R}_{\text{PTF}}(\theta_i))$  (11)
4:      $\Omega \leftarrow \text{SKEWMATRIX}(\boldsymbol{\omega}_{\text{PTF}}(\theta_i))$  (5)
5:      $\Delta\theta = \theta_{i+1} - \theta_i$ 
6:      $\mathbf{R}_{\text{PTF}}(\theta_{i+1}) \leftarrow \text{INTEGRATE}(\mathbf{R}_{\text{PTF}}(\theta_i), \Omega, \Delta\theta)$  (12)
7:   end for
8:   return  $\mathbf{R}_{\text{PTF}}(\theta_0, \dots, \theta_N), \boldsymbol{\omega}_{\text{PTF}}(\theta_0, \dots, \theta_N)$ 
9: end function

```

Having obtained the PTF components \mathbf{R}_{PTF} and angular velocity $\boldsymbol{\omega}_{\text{PTF}}$, we can now proceed to computing the respective higher derivatives. Given that differentiable path-parametric methods require from first order (learning) and second order (optimization) gradients, we will focus on the derivation of the first two derivatives. However, the suggested methodology can be extended to higher order derivatives by following the same procedure.

Starting with the first order derivatives, \mathbf{R}_{PTF} is readily available from (5) and (11), while the angular acceleration $\boldsymbol{\alpha}_{\text{PTF}}$ can be obtained by derivating (11):

$$\boldsymbol{\alpha}_{\text{PTF}}(\theta) = \boldsymbol{\alpha}_{\text{PTF}}^{\Gamma}(\theta)\mathbf{R}_{\text{PTF}}^{\top}(\theta) + \boldsymbol{\omega}_{\text{PTF}}^{\Gamma}(\theta)\mathbf{R}_{\text{PTF}}^{\top}(\theta) \quad (13a)$$

with

$$\boldsymbol{\alpha}_{\text{PTF}}^{\Gamma}(\theta) = \left[0, -\left(\mathbf{e}''_1(\theta)\mathbf{e}_3(\theta) + \mathbf{e}'_1(\theta)\mathbf{e}'_3(\theta)\right), \mathbf{e}''_1(\theta)\mathbf{e}_2(\theta) + \mathbf{e}'_1(\theta)\mathbf{e}'_2(\theta)\right]. \quad (13b)$$

To derive the second derivative of the moving frame $\mathbf{R}_{\text{PTF}}''$, we express the angular velocity (11) and acceleration (13) by their skew-symmetric matrices $\Omega_{\text{PTF}}, \Omega'_{\text{PTF}}$ and combine them with the derivative of (5) over θ , which results in:

$$\mathbf{R}_{\text{PTF}}'' = \Omega'_{\text{PTF}}(\theta)\mathbf{R}_{\text{PTF}}(\theta) + \Omega_{\text{PTF}}(\theta)\mathbf{R}'_{\text{PTF}}(\theta) \quad (14)$$

Finally, to calculate the second derivative of the angular velocity –denoted as angular jerk \mathbf{j}_Γ – we derivate (13):

$$\mathbf{j}_{\text{PTF}}^\Gamma(\theta) = \mathbf{j}_{\text{PTF}}^\Gamma(\theta) \mathbf{R}_{\text{PTF}}^\Gamma(\theta) + \boldsymbol{\alpha}_{\text{PTF}}^\Gamma(\theta) \mathbf{R}_{\text{PTF}}^{\prime\Gamma}(\theta) + \boldsymbol{\alpha}_{\text{PTF}}^\Gamma(\theta) \mathbf{R}_{\text{PTF}}^{\prime\Gamma}(\theta) + \boldsymbol{\omega}_{\text{PTF}}^\Gamma(\theta) \mathbf{R}_{\text{PTF}}^{\prime\prime\Gamma}(\theta), \quad (15a)$$

where

$$\mathbf{j}_{\text{PTF}}^\Gamma(\theta) = \left[0, - \left(\mathbf{e}_1'''(\theta) \mathbf{e}_3(\theta) + \mathbf{e}_1''(\theta) \mathbf{e}_3'(\theta) + \mathbf{e}_1''(\theta) \mathbf{e}_3'(\theta) + \mathbf{e}_1'(\theta) \mathbf{e}_3''(\theta) \right), \right. \\ \left. \mathbf{e}_1'''(\theta) \mathbf{e}_2(\theta) + \mathbf{e}_1''(\theta) \mathbf{e}_2'(\theta) + \mathbf{e}_1'(\theta) \mathbf{e}_2''(\theta) + \mathbf{e}_1'(\theta) \mathbf{e}_2''(\theta) \right]. \quad (15b)$$

Eqs. (11), (13), (15) show how the continuity of the reference path $\gamma(\theta)$ and angular frame $\boldsymbol{\omega}(\xi)$ are related:

$$\mathbf{e}_1'(\theta), \mathbf{R}_{\text{PTF}}(\theta) \rightarrow \boldsymbol{\omega}_{\text{PTF}}(\theta), \quad (16a)$$

$$\mathbf{e}_1''(\theta), \mathbf{R}_{\text{PTF}}(\theta), \mathbf{R}_{\text{PTF}}'(\theta) \rightarrow \boldsymbol{\alpha}_{\text{PTF}}(\theta), \quad (16b)$$

$$\mathbf{e}_1'''(\theta), \mathbf{R}_{\text{PTF}}(\theta), \mathbf{R}_{\text{PTF}}'(\theta), \mathbf{R}_{\text{PTF}}''(\theta) \rightarrow \mathbf{j}_{\text{PTF}}(\theta), \quad (16c)$$

i.e., a path with continuity degree $\gamma \in C^n$ relates to $\mathbf{R}_{\text{PTF}} \in C^{n-1}$ and $\boldsymbol{\omega}_{\text{PTF}} \in C^{n-2}$. For example, if we desire $\boldsymbol{\omega}_{\text{PTF}}$ to be C^2 , γ needs to be (at least) C^4 . The specific steps necessary for computing the first and second order derivatives of the moving frame components and angular velocity are detailed in Algorithm 2.

In summary, Algorithms 1 and 2 facilitate the computation of the moving frame \mathbf{R}_{RMF} , angular velocity $\boldsymbol{\omega}_{\text{RMF}}$ and its derivatives $\{\mathbf{R}_{\text{RMF}}', \mathbf{R}_{\text{RMF}}'', \boldsymbol{\alpha}_{\text{RMF}}, \mathbf{j}_{\text{RMF}}\}$. This combination of accessibility and efficiency, along with the inherent advantages of the PTFs — namely, being singularity-free and twist-free — renders the proposed moving frame computation method highly suitable for path-parametric planning and control algorithms.

Algorithm 2 *Parallel Transport Frame Derivatives (PTFD):*

Input: $\mathbf{R}_{\text{PTF}}(\theta_0, \dots, \theta_N)$, $\boldsymbol{\omega}_{\text{PTF}}(\theta_0, \dots, \theta_N)$, $\mathbf{e}_1'(\theta_0, \dots, \theta_N)$, $\mathbf{e}_1''(\theta_0, \dots, \theta_N)$, $\mathbf{e}_1'''(\theta_0, \dots, \theta_N)$

Output: $\mathbf{R}_{\text{PTF}}'(\theta_0, \dots, \theta_N)$, $\mathbf{R}_{\text{PTF}}''(\theta_0, \dots, \theta_N)$, $\boldsymbol{\alpha}_{\text{PTF}}(\theta_0, \dots, \theta_N)$, $\mathbf{j}_{\text{PTF}}(\theta_0, \dots, \theta_N)$

```

1: function PTFD( $\mathbf{R}_{\text{PTF}}(\theta_0, \dots, \theta_N)$ ,  $\boldsymbol{\omega}_{\text{PTF}}(\theta_0, \dots, \theta_N)$ )
2:   for  $i \in \{0, \dots, N\}$  do
3:      $\mathbf{R}_{\text{PTF}}'(\theta_i) \leftarrow \text{FRAMEVEL}(\mathbf{R}_{\text{PTF}}(\theta_i), \boldsymbol{\omega}_{\text{PTF}}(\theta_i))$  (5)
4:      $\boldsymbol{\alpha}_{\text{PTF}}(\theta_i) \leftarrow \text{ANGULARACC}(\mathbf{e}_1''(\theta_i), \mathbf{R}_{\text{PTF}}(\theta_i), \mathbf{R}_{\text{PTF}}'(\theta_i))$  (13)
5:      $\mathbf{R}_{\text{PTF}}''(\theta_i) \leftarrow \text{FRAMEACC}(\mathbf{R}_{\text{PTF}}(\theta_i), \boldsymbol{\omega}_{\text{PTF}}(\theta_i), \boldsymbol{\alpha}_{\text{PTF}}(\theta_i))$  (14)
6:      $\mathbf{j}_{\text{PTF}}(\theta_i) \leftarrow \text{ANGULARJERK}(\mathbf{e}_1'''(\theta_i), \mathbf{R}_{\text{PTF}}(\theta_i), \mathbf{R}_{\text{PTF}}'(\theta_i), \mathbf{R}_{\text{PTF}}''(\theta_i))$  (15)
7:   end for
8:   return  $\mathbf{R}_{\text{PTF}}'(\theta_0, \dots, \theta_N)$ ,  $\mathbf{R}_{\text{PTF}}''(\theta_0, \dots, \theta_N)$ ,  $\boldsymbol{\alpha}_{\text{PTF}}(\theta_0, \dots, \theta_N)$ ,  $\mathbf{j}_{\text{PTF}}(\theta_0, \dots, \theta_N)$ 
9: end function

```

3.4 Numerical tests

To showcase the concepts presented in this section, we provide two numerical tests: First, we compare the FSF to the PTF for a two-dimensional planar curve and a three-dimensional spatial curve. Second, we observe how the continuity of the reference path and the angular velocity of the moving frames are related.

Comparing Frenet-Serret (FSF) against Parallel-Transport (PTF)

In Fig. 2 we show a 2D (top row) and 3D (bottom row) comparison between the FSF (first column) and the PTF (second column). The planar comparison is based on the curve $\gamma(\theta) = [\gamma, \sin(2\pi\theta)]$ and clearly depicts how the FSF presents a singularity in the inflection point, where the frame is not defined and its normal component abruptly flips. The spatial curve relates to the curve $\gamma(\theta) = [(0.6 + 0.3 \cos(\theta)) \cos(2\theta), (0.6 + 0.3 \cos(\theta)) \sin(2\theta), 0.3 \sin(7\theta)]$ and showcases how the FSF presents an undesired rotation over its first component. In contrast, the PTF does not suffer from this twist, ultimately leading to a moving frame with a lower angular velocity magnitude (third column).

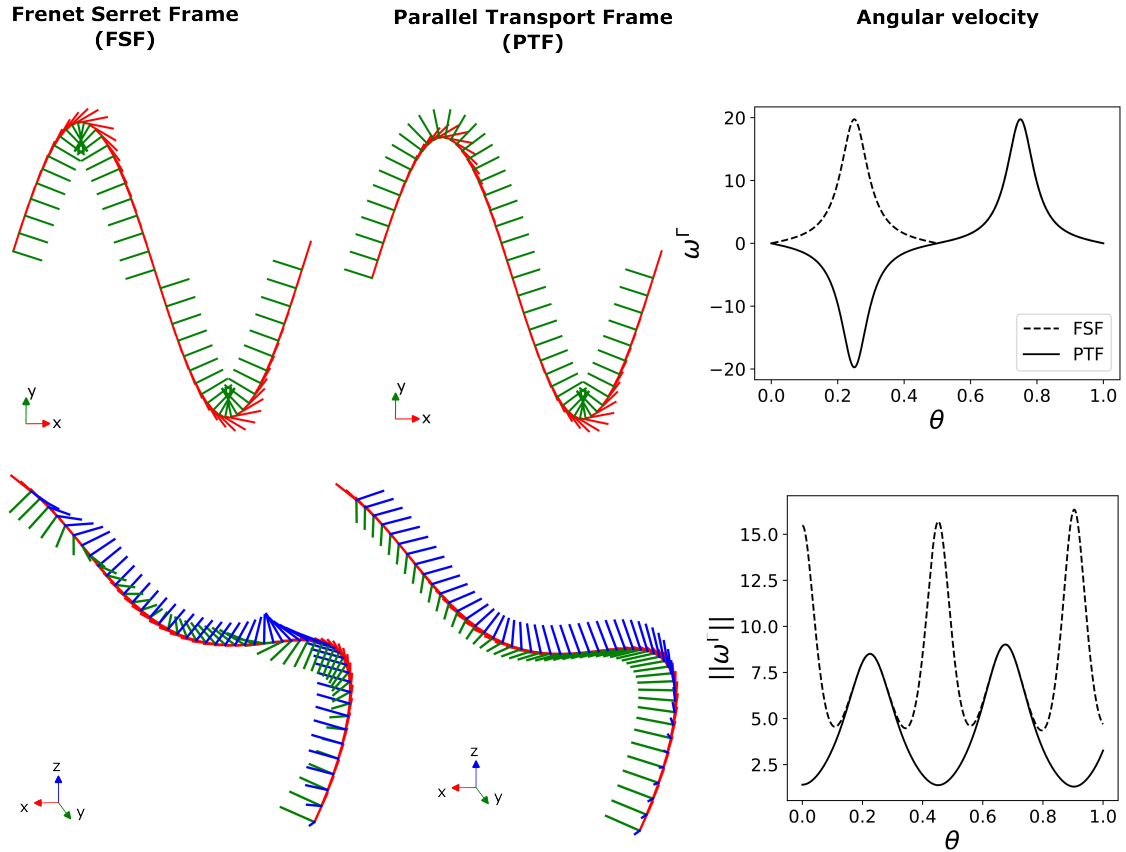


Figure 2: Comparison of Frenet Serret Frame (FSF, first column) and Parallel Transport Frame (PTF, second column) for a two-dimensional planar curve (first row) and three-dimensional spatial curve (second row). The first, second and third components of the moving frame are shown in red, green and blue, respectively. The third column shows the angular velocity of the moving frames.

Continuity in the angular velocity

In eqs. (16) it was concluded that a reference path γ that is C^n relates to an angular velocity ω_{PTF} that is C^{n-2} . To numerically validate this statement, we divide an illustrative curve $\gamma(\theta) = [0.5 \cos(9\theta), e^{\cos(1.8\theta)}]$ into two sections, conduct interpolations of different degrees and observe the continuity of the angular velocity. The obtained results are shown in Fig. 3 and confirm the theoretical analysis: When the interpolation is C^2 , the angular velocity is C^0 (only ω_{PTF} is continuous); when the interpolation is C^3 , the angular velocity is C^1 ($\omega_{\text{PTF}}, \alpha_{\text{PTF}}$ are continuous); and when the interpolation is C^4 , the angular velocity is C^2 ($\omega_{\text{PTF}}, \alpha_{\text{PTF}}, \mathbf{j}_{\text{PTF}}$ are continuous).

4 Path parameterizing the Cartesian coordinates

In this section, we concentrate on the second ingredient of the universal framework, specifically a parametric reformulation that projects the Cartesian system dynamics into the spatial states associated with a parametric path. This is addressed in three distinct steps: First, we formally define the spatial states, as an alternative representation of the Cartesian coordinates. Second, we derive the equations of motion for this representation without making any assumptions regarding the underlying path parameterization. This ensures full compliance with the methods outlined in the previous section and demonstrates that existing formulations in the literature are specific cases of the presented derivation. Lastly, we discuss how the parametric terms required by the derived equations of motion seamlessly integrate with the algorithms introduced in the previous section.

4.1 Spatial states: An alternative to Cartesian coordinates

We consider continuous time, (non)linear dynamic systems of the form

$$\dot{\mathbf{x}}(t) = f(\mathbf{x}(t), \mathbf{u}(t)), \quad (17a)$$

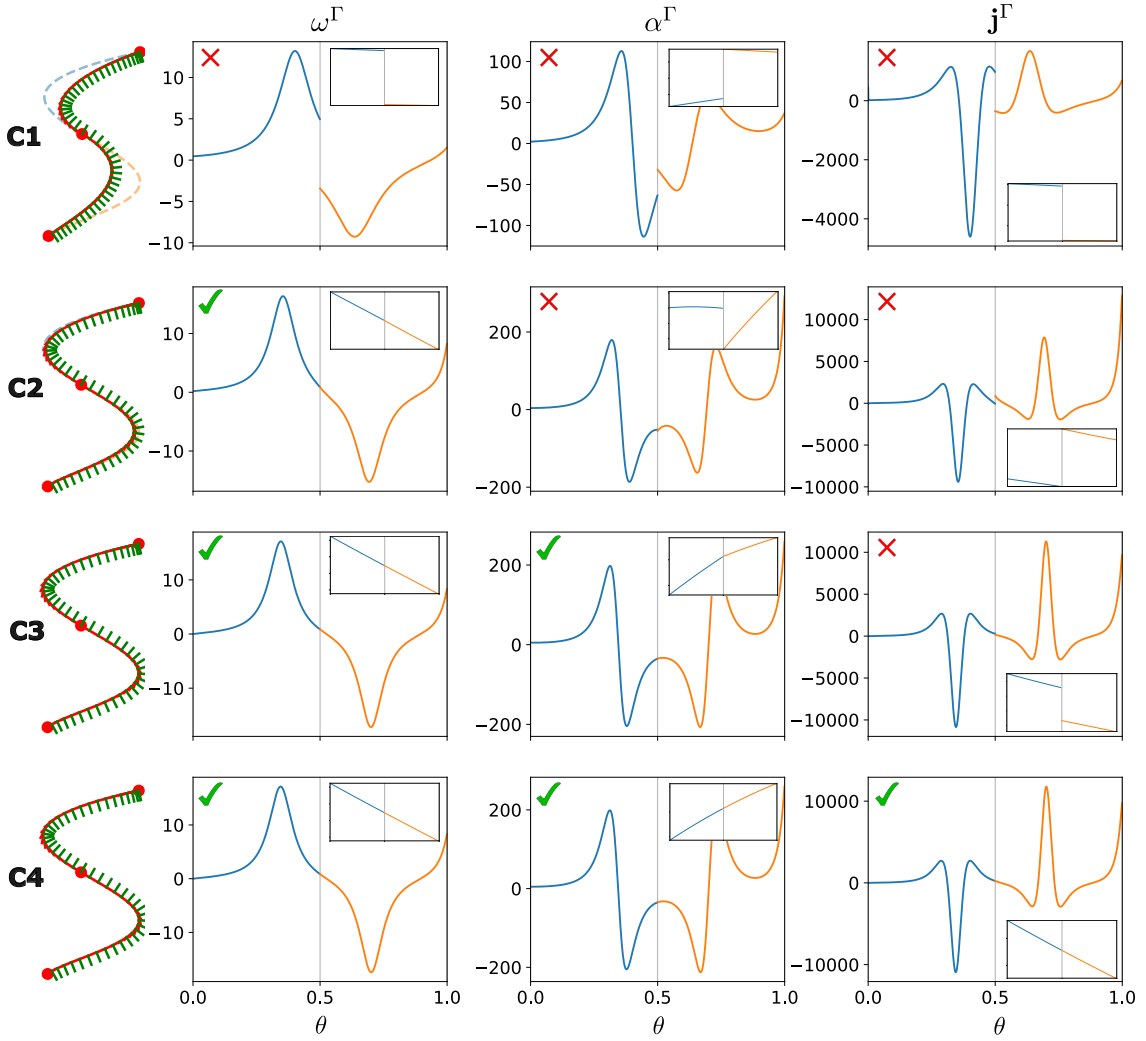


Figure 3: Numerical validation of the continuity analysis conducted in eqs. (16), namely that a reference curve γ that is C^n relates to an angular velocity ω_{PTF} that is C^{n-2} . For this purpose we divide an exemplary curve into two sections and interpolate with various continuity degree (C^0 to C^4 from top to bottom). The left column shows the exemplary curve, while the remaining columns depict the angular velocity ω^Γ , acceleration α^Γ and jerk j^Γ . The intersection is given by the red dot located in the middle of the curve at $\theta = 0.5$. The evaluations associated to the first and second sections are depicted in blue and orange. The boxes in the upper right side of each plot provide a more detailed look into the intersection, allowing us to differ the continuous and discontinuous cases. Additionally, the continuous cases have been labelled by a green tick, while the discontinuous ones are marked by a red cross.

where $\mathbf{x} \in \mathbb{R}^{n_x}$ and $\mathbf{u} \in \mathbb{R}^{n_u}$ define the system states and inputs, respectively. We assume that the Cartesian coordinates $\mathbf{p}^W(t) \in \mathbb{R}^3$ associated to the system's longitudinal location with respect to a world-frame $(\cdot)_W$ in the Euclidean space are given by a (non)linear mapping h , such that

$$\mathbf{p}^W(t) = h(\mathbf{x}(t)). \quad (17b)$$

To project the system dynamics (17a) onto the reference Γ in (3), we introduce the *spatial coordinates* as an alternative to the Cartesian representation in (17b). For this purpose, we decouple the system's translational motion into two terms: a *tangent* element – describing the progress along the path – and a *transverse* component – representing the distance perpendicular to the path –.

Given the dynamical system's Cartesian location $\mathbf{p}^W(t)$ in (17b), we define the *progress variable* $\xi(t)$ as the path parameter θ of the closest point in the reference Γ , i.e.,

$$\xi(t) = \theta^*(t) = \arg \min_{\theta} \frac{1}{2} \|\mathbf{p}^W(t) - \gamma(\theta)\|^2. \quad (18)$$

An explicit representation of the progress variable $\xi(t)$ as in (18) allows for expressing the distance

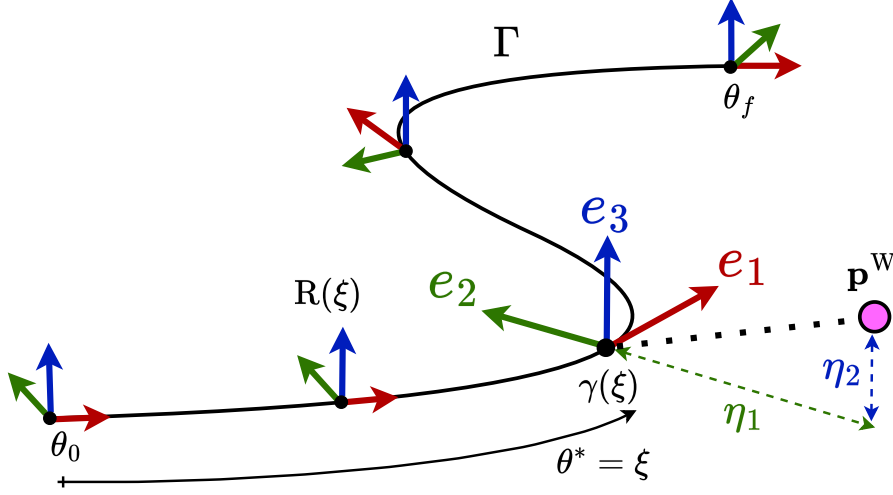


Figure 4: Spatial projection of the three-dimensional Cartesian coordinates \mathbf{p}^W , represented by the pink dot, onto a geometric path Γ with an associated adapted-frame $R(\xi) = \{\mathbf{e}_1(\xi), \mathbf{e}_2(\xi), \mathbf{e}_3(\xi)\}$. The distance to the closest point on the path $\gamma(\xi)$ is decomposed into the transverse coordinates $\boldsymbol{\eta} = [\eta_1, \eta_2]$.

between the dynamical system and the reference path, in both the world-frame and the path-frame:

$$\mathbf{d}^\Gamma(t) = R(\xi(t))^\top \mathbf{d}^W(t) \quad \text{with} \quad \mathbf{d}^W(t) = \mathbf{p}^W(t) - \gamma(\xi(t)). \quad (19)$$

Since we have assumed the path-frame $R(\xi(t))$ to be adapted, the first element of $\mathbf{d}^\Gamma(t)$, is zero, while the remaining two are the perpendicular projections, which refer to the aforementioned transverse component $\boldsymbol{\eta}(t) = [\eta_1(t), \eta_2(t)]$. Consequently, eq. (19) simplifies into

$$\mathbf{d}^\Gamma(t) = [0, \boldsymbol{\eta}(t)] = [0, \mathbf{e}_2(\xi(t))\mathbf{d}^W(t), \mathbf{e}_3(\xi(t))\mathbf{d}^W(t)]^\top. \quad (20)$$

Finally, combining the progress variable $\xi(t)$ in (18) with the transverse coordinates $\boldsymbol{\eta}(t)$ in (20), we define the *spatial coordinates* as an alternative representation for the location of the dynamical system (17) in the Euclidean space:

$$\mathbf{p}^\Gamma(t) = [\xi(t), \boldsymbol{\eta}(t)] \in \mathbb{R}^3 \quad (21)$$

For an illustrative visualization of the spatial coordinates associated to the reference path Γ , please refer to Fig. 4.

4.2 Derivation of equations of motion

Given the dynamical system in (17) and the parametric reference path Γ in (3), we derive the equations of motion for the spatial coordinates in (21). To conduct this derivation, we offer two distinct approaches: one based on kinematics and another rooted in optimality principles.

A kinematic derivation

From the distances in (19) the Cartesian coordinates of the dynamical system (17) can be expressed as

$$\mathbf{p}^W(t) = \gamma(\xi(t)) + R(\xi(t))\mathbf{d}^\Gamma(t) \quad (22)$$

Differentiating (22) with respect to time results in

$$\mathbf{v}^W(t) = \dot{\xi}(t) (\boldsymbol{\gamma}'(\xi(t)) + R'(\xi(t))\mathbf{d}^\Gamma(t)) + R(\xi(t))\dot{\mathbf{d}}^\Gamma(t). \quad (23)$$

Denoting $\mathbf{i}^W = [1, 0, 0]^\top$ as the first component of the world-frame and, recalling from (2) that the curve's parametric speed is $\sigma(\xi(t)) = \|\boldsymbol{\gamma}'(\xi(t))\|$, we can derive:

$$\boldsymbol{\gamma}'(\xi(t)) \equiv \sigma(\xi(t))\mathbf{e}_1(\xi(t)) \equiv R(\xi(t))\mathbf{i}^W\sigma(\xi(t)). \quad (24)$$

Introducing (24) in (23) and multiplying it with $\mathbf{R}^\top(\xi(t))$ leads to

$$0 = \dot{\xi}(t) \left(\sigma(\xi(t)) \mathbf{i}^W + \mathbf{R}(\xi(t))^\top \mathbf{R}'(\xi(t)) \mathbf{d}^\Gamma(\xi(t)) \right) + \mathbf{d}^\Gamma(t) - \mathbf{R}^\top(\xi(t)) \mathbf{v}^W(t).$$

Leveraging the skew symmetric matrix in (5), the latter equation can be simplified to

$$0 = \dot{\xi}(t) \left(\sigma(\xi(t)) \mathbf{i}^W + \Omega^\Gamma(\xi(t)) \mathbf{d}^\Gamma(\xi(t)) \right) + \mathbf{d}^\Gamma(t) - \mathbf{R}^\top(\xi(t)) \mathbf{v}^W(t),$$

which combined with (5) and (19), finally yields the equations of motion for the *spatial coordinates*:

Model 1 (Path-parameterized Cartesian motion): *The motion of a three-dimensional point moving at speed $\mathbf{v}^W(t)$ with respect to a reference path parameterized by $\xi(t)$ with parametric speed $\sigma(\xi(t))$ and an adapted path-frame $\mathbf{R}(\xi) = [\mathbf{e}_1(\xi(t)), \mathbf{e}_2(\xi(t)), \mathbf{e}_3(\xi(t))]$ whose angular velocity is $\boldsymbol{\omega}(\xi(t)) = \omega_1^\Gamma(\xi(t)) \mathbf{e}_1(\xi(t)) + \omega_2^\Gamma(\xi(t)) \mathbf{e}_2(\xi(t)) + \omega_3^\Gamma(\xi(t)) \mathbf{e}_3(\xi(t))$ is given by the following equations:*

$$\dot{\xi}(t) = \frac{\mathbf{e}_1(\xi(t))^\top \mathbf{v}^W(t)}{\sigma(\xi(t)) - \omega_3^\Gamma(\xi(t)) \eta_1(t) + \omega_2^\Gamma(\xi(t)) \eta_2(t)}, \quad (25a)$$

$$\dot{\eta}_1(t) = \mathbf{e}_2(\xi(t))^\top \mathbf{v}^W(t) + \dot{\xi}(t) \omega_1^\Gamma(\xi(t)) \eta_2(t), \quad (25b)$$

$$\dot{\eta}_2(t) = \mathbf{e}_3(\xi(t))^\top \mathbf{v}^W(t) - \dot{\xi}(t) \omega_1^\Gamma(\xi(t)) \eta_1(t). \quad (25c)$$

An optimality derivation

In here we show that an alternative approach also allows for the derivation of the equations of motion in (25). More specifically, we focus on the original definition of the progress variable $\xi(t)$ in (18). Given that this is an unconstrained optimization, we leverage the first order optimality condition, so that

$$0 = \frac{d}{d\theta} \left(\frac{1}{2} \|\mathbf{p}^W(t) - \boldsymbol{\gamma}(\theta)\|^2 \right), \quad (26)$$

which for the optimal path parameter $\theta^*(t) = \xi(t)$ results in

$$0 = (\mathbf{p}^W(t) - \boldsymbol{\gamma}(\xi(t))) \boldsymbol{\gamma}'(\xi(t)).$$

Similarly, we enforce the first optimality condition with respect to time, i.e.,

$$0 = \frac{d}{dt} \left((\mathbf{p}^W(t) - \boldsymbol{\gamma}(\xi(t))) \boldsymbol{\gamma}'(\xi(t)) \right),$$

whose expansion is

$$0 = \mathbf{v}^W(t) \boldsymbol{\gamma}'(\xi(t)) - \dot{\xi}(t) \boldsymbol{\gamma}'(\xi(t)) \boldsymbol{\gamma}'(\xi(t)) + \dot{\xi}(t) (\mathbf{p}^W(t) - \boldsymbol{\gamma}(\xi(t))) \boldsymbol{\gamma}''(\xi(t)).$$

Noticing that $\sigma^2(\xi(t)) = \boldsymbol{\gamma}'(\xi(t)) \boldsymbol{\gamma}'(\xi(t))$ the equation above simplifies to

$$\dot{\xi}(t) = \frac{\mathbf{v}^W(t) \boldsymbol{\gamma}'(\xi(t))}{\sigma^2(\xi(t)) - \mathbf{d}^W(t) \boldsymbol{\gamma}''(\xi(t))}. \quad (27)$$

Recalling that $\mathbf{e}_1(\xi(t)) = \frac{\boldsymbol{\gamma}(\xi(t))}{\sigma(\xi(t))}$, follows that $\boldsymbol{\gamma}''(\xi(t)) = \mathbf{e}_1'(\xi(t)) \sigma(\xi(t)) + \mathbf{e}_1(\xi(t)) \sigma'(\xi(t))$, whose derivative in the first term is known from (5), i.e., $\mathbf{e}_1'(\xi(t)) = \mathbf{e}_2(\xi(t)) \omega_3^\Gamma(\xi(t)) - \mathbf{e}_3(\xi(t)) \omega_2^\Gamma(\xi(t))$ and second term gets cancelled because $\mathbf{d}^W(t)$ is perpendicular to $\mathbf{e}_1(\xi(t))$. Incorporating this information into (27) results in

$$\dot{\xi}(t) = \frac{\mathbf{v}^W(t) \boldsymbol{\gamma}'(\xi(t))}{\sigma^2(\xi(t)) - \sigma(\xi(t)) \mathbf{d}^W(t) (\mathbf{e}_2(\xi(t)) \omega_3^\Gamma(\xi(t)) - \mathbf{e}_3(\xi(t)) \omega_2^\Gamma(\xi(t)))}. \quad (28)$$

and dividing both the numerator and denominator by $\sigma(\xi(t))$ and combining it with (20), coincides with (25a), the equation of motion for the progress variable $\xi(t)$ derived by the previous kinematic approach. The remaining equations of motions for the transverse coordinates $\boldsymbol{\eta}(t)$ (25b) and (25c), can easily be obtained from derivating (20) on time and following similar simplifications as above.

4.3 A universal path-parameterization

The equations of motion for the spatial states derived in (25) are universal, as they do not rely on any assumptions regarding the underlying path parameterization. In other words, they are applicable to any parametric path, regardless of its parametric speed and moving frame. To showcase this universality, we demonstrate how the well-known Frenet-Serret based parametric model is a particular instance of the equations of motion in (25). Additionally, we show how the two-dimensional case, relevant for planar application such as autonomous driving, is a trivial simplification of the three-dimensional one.

A particular case: The Frenet Serret based models

The analytical simplicity and ease of implementation make the FSF the most widely applied moving frame in literature [1, 13, 33]. This spread is rooted in the autonomous driving community [29, 36, 40], where the planar application of the FSF allows for numerical tricks to dodge its fundamental limitations. This influence, combined with the aforementioned simplicity, have made the FSF the de facto standard for path-parametric planning and control, even for three-dimensional applications [2, 9, 42], where the FSF suffers from all the limitations discussed in Section 3. As a consequence, the parametric formulations available in the literature are specific to the FSF. To show this, it is sufficient to tailor eqs. (25) by specifying the angular velocity as in (8) i.e., $[\omega_1^T, \omega_2^T, \omega_3^T] = \sigma [\tau, 0, \kappa]$. Furthermore, if the curve is assumed to be parameterized directly by its arc-length $L = \xi$, the parametric speed reduces to a unit magnitude $\sigma(\xi) = \frac{dL}{d\xi} = 1$:

$$\dot{\xi}(t) = \frac{\mathbf{e}_1(\xi(t))^T \mathbf{v}^W(t)}{1 - \kappa(\xi(t))\eta_1(t)}, \quad (29a)$$

$$\dot{\eta}_1(t) = \mathbf{e}_2(\xi(t))^T \mathbf{v}^W(t) + \dot{\xi}(t)\tau(\xi(t))\eta_2(t), \quad (29b)$$

$$\dot{\eta}_2(t) = \mathbf{e}_3(\xi(t))^T \mathbf{v}^W(t) - \dot{\xi}(t)\tau(\xi(t))\eta_1(t). \quad (29c)$$

The resultant equations of motion are specific to the FSF and match the ones available in literature, e.g. [1, 13], showcasing the generality of our equations in (25).

The planar 2D case

In the case of planar motions, such as ground vehicles, the parameterization in (25) simplifies to two states, i.e., the second component of the transverse components gets cancelled $\eta_2(t) = 0$. Consequently, the equations of motion in (25) reduce to the following planar model:

$$\dot{\xi}(t) = \frac{\mathbf{e}_1(\xi(t))^T \mathbf{v}^W(t)}{\sigma(\xi(t)) - \omega_3^T(\xi(t))\eta_1(t)}, \quad (30a)$$

$$\dot{\eta}_1(t) = \mathbf{e}_2(\xi(t))^T \mathbf{v}^W(t). \quad (30b)$$

In a similar way as for the three-dimensional case, the planar model can be tailored to the FSF by specifying the angular velocity as in (8) and the parametric speed as $\sigma(\xi) = 1$. This results in the following planar model:

$$\dot{\xi}(t) = \frac{\mathbf{e}_1(\xi(t))^T \mathbf{v}^W(t)}{1 - \kappa(\xi(t))\eta_1(t)}, \quad (31a)$$

$$\dot{\eta}_1(t) = \mathbf{e}_2(\xi(t))^T \mathbf{v}^W(t), \quad (31b)$$

which is commonly employed in the autonomous driving community.

4.4 Modularity: Frames and Equations

Before concluding this section, there are two points that we would like to emphasize: First, the equations derived in (25) are universal, in the sense that they can be used alongside any moving frame and path-parameterization technique. For example, in the previous subsection we have tailored them for the FSF case. To shed some light on the choice of the moving frame, in Section 3 we presented the PTF as the most suitable candidate. It goes without saying that Algorithms 1 and 2 interplay perfectly with the equations of motion in (25). The fusion of the PTF and the universal equations of motion is a powerful formulation, that enjoys the benefits of both ingredients.

The second point is to recognize that, despite our best efforts, we – the authors – might have failed to identify the most appropriate frame and parameterization technique. It is very likely that

future researchers will come up with more appropriate methods to define and compute moving frames. Despite this, it is important to insist that the equations of motion in (25) still remain relevant. The presented universal framework is modular in the sense that the underlying ingredients are completely decoupled, i.e., the path parameterization technique is agnostic to the equations of motion of the spatial states. Therefore, even if future research leads to the development of more suitable moving frames, they can still be used alongside the equations of motion in (25).

References

- [1] R. Verschueren, N. van Duijkeren, J. Swevers, and M. Diehl, “Time-optimal motion planning for n-dof robot manipulators using a path-parametric system reformulation,” in *2016 American Control Conference (ACC)*, pp. 2092–2097, IEEE, 2016.
- [2] S. Spedicato and G. Notarstefano, “Minimum-time trajectory generation for quadrotors in constrained environments,” *IEEE Transactions on Control Systems Technology*, vol. 26, no. 4, pp. 1335–1344, 2017.
- [3] J. Arrizabalaga and M. Ryll, “Sctomp: Spatially constrained time-optimal motion planning,” in *2023 IEEE/RSJ International Conference on Intelligent Robots and Systems (IROS)*, pp. 4827–4834, IEEE, 2023.
- [4] Y. Song, M. Steinweg, E. Kaufmann, and D. Scaramuzza, “Autonomous drone racing with deep reinforcement learning,” in *2021 IEEE/RSJ International Conference on Intelligent Robots and Systems (IROS)*, pp. 1205–1212, IEEE, 2021.
- [5] P. R. Wurman, S. Barrett, K. Kawamoto, J. MacGlashan, K. Subramanian, T. J. Walsh, R. Capobianco, A. Devlic, F. Eckert, F. Fuchs, *et al.*, “Outracing champion gran turismo drivers with deep reinforcement learning,” *Nature*, vol. 602, no. 7896, pp. 223–228, 2022.
- [6] E. Kaufmann, L. Bauersfeld, A. Loquercio, M. Müller, V. Koltun, and D. Scaramuzza, “Champion-level drone racing using deep reinforcement learning,” *Nature*, vol. 620, no. 7976, pp. 982–987, 2023.
- [7] A. Liniger, A. Domahidi, and M. Morari, “Optimization-based autonomous racing of 1: 43 scale rc cars,” *Optimal Control Applications and Methods*, vol. 36, no. 5, pp. 628–647, 2015.
- [8] T. Oelerich, F. Beck, C. Hartl-Nesic, and A. Kugi, “Boundmpc: Cartesian trajectory planning with error bounds based on model predictive control in the joint space,” *arXiv preprint arXiv:2401.05057*, 2024.
- [9] J. Arrizabalaga and M. Ryll, “Towards time-optimal tunnel-following for quadrotors,” in *2022 International Conference on Robotics and Automation (ICRA)*, pp. 4044–4050, IEEE, 2022.
- [10] D. Lam, C. Manzie, and M. Good, “Model predictive contouring control,” in *49th IEEE Conference on Decision and Control (CDC)*, pp. 6137–6142, IEEE, 2010.
- [11] T. Faulwasser and R. Findeisen, “Nonlinear model predictive control for constrained output path following,” *IEEE Transactions on Automatic Control*, vol. 61, no. 4, pp. 1026–1039, 2015.
- [12] D. Verscheure, B. Demeulenaere, J. Swevers, J. De Schutter, and M. Diehl, “Time-optimal path tracking for robots: A convex optimization approach,” *IEEE Transactions on Automatic Control*, vol. 54, no. 10, pp. 2318–2327, 2009.
- [13] N. van Duijkeren, R. Verschueren, G. Pipeleers, M. Diehl, and J. Swevers, “Path-following nmpc for serial-link robot manipulators using a path-parametric system reformulation,” in *2016 European Control Conference (ECC)*, pp. 477–482, IEEE, 2016.
- [14] J. Arrizabalaga and M. Ryll, “Spatial motion planning with pythagorean hodograph curves,” in *2022 IEEE 61st Conference on Decision and Control (CDC)*, pp. 2047–2053, IEEE, 2022.
- [15] “The history of curvature.” https://web.archive.org/web/20071106083431/http://www3.villanova.edu/maple/misc/history_of_curvature/k.htm. Accessed: 2024-05-27.
- [16] J. M. Hollerbach, “Dynamic scaling of manipulator trajectories,” in *1983 American Control Conference*, pp. 752–756, IEEE, 1983.
- [17] K. Shin and N. McKay, “Minimum-time control of robotic manipulators with geometric path constraints,” *IEEE Transactions on Automatic Control*, vol. 30, no. 6, pp. 531–541, 1985.
- [18] F. Pfeiffer and R. Johanni, “A concept for manipulator trajectory planning,” *IEEE Journal on Robotics and Automation*, vol. 3, no. 2, pp. 115–123, 1987.
- [19] W. L. Nelson and I. J. Cox, “Local path control for an autonomous vehicle,” in *Proceedings. 1988 IEEE International Conference on Robotics and Automation*, pp. 1504–1510, IEEE, 1988.

- [20] Y. Kanayama, Y. Kimura, F. Miyazaki, and T. Noguchi, “A stable tracking control method for an autonomous mobile robot,” in *Proceedings., IEEE International Conference on Robotics and Automation*, pp. 384–389, IEEE, 1990.
- [21] I. J. Cox, “Blanche—an experiment in guidance and navigation of an autonomous robot vehicle,” *IEEE Transactions on robotics and automation*, vol. 7, no. 2, pp. 193–204, 1991.
- [22] J. Hauser and R. Hindman, “Maneuver regulation from trajectory tracking: Feedback linearizable systems,” *IFAC Proceedings Volumes*, vol. 28, no. 14, pp. 595–600, 1995.
- [23] R. Skjetne, T. I. Fossen, and P. V. Kokotović, “Robust output maneuvering for a class of nonlinear systems,” *Automatica*, vol. 40, no. 3, pp. 373–383, 2004.
- [24] K. D. Do, Z.-P. Jiang, and J. Pan, “Robust adaptive path following of underactuated ships,” *Automatica*, vol. 40, no. 6, pp. 929–944, 2004.
- [25] A. P. Aguiar, J. P. Hespanha, and P. V. Kokotovic, “Path-following for nonminimum phase systems removes performance limitations,” *IEEE Transactions on Automatic Control*, vol. 50, no. 2, pp. 234–239, 2005.
- [26] A. P. Aguiar and J. P. Hespanha, “Trajectory-tracking and path-following of underactuated autonomous vehicles with parametric modeling uncertainty,” *IEEE transactions on automatic control*, vol. 52, no. 8, pp. 1362–1379, 2007.
- [27] T. Faulwasser, B. Kern, and R. Findeisen, “Model predictive path-following for constrained nonlinear systems,” in *Proceedings of the 48th IEEE Conference on Decision and Control (CDC) held jointly with 2009 28th Chinese Control Conference*, pp. 8642–8647, IEEE, 2009.
- [28] F. Kehrle, J. V. Frasch, C. Kirches, and S. Sager, “Optimal control of formula 1 race cars in a vdrift based virtual environment,” *IFAC Proceedings Volumes*, vol. 44, no. 1, pp. 11907–11912, 2011.
- [29] Y. Gao, A. Gray, J. V. Frasch, T. Lin, E. Tseng, J. K. Hedrick, and F. Borrelli, “Spatial predictive control for agile semi-autonomous ground vehicles,” in *Proceedings of the 11th international symposium on advanced vehicle control*, no. 2, pp. 1–6, 2012.
- [30] T. Faulwasser, J. Matschek, P. Zometa, and R. Findeisen, “Predictive path-following control: Concept and implementation for an industrial robot,” in *2013 IEEE International Conference on Control Applications (CCA)*, pp. 128–133, IEEE, 2013.
- [31] J. V. Frasch, A. Gray, M. Zanon, H. J. Ferreau, S. Sager, F. Borrelli, and M. Diehl, “An auto-generated nonlinear mpc algorithm for real-time obstacle avoidance of ground vehicles,” in *2013 European Control Conference (ECC)*, pp. 4136–4141, IEEE, 2013.
- [32] M. Böck and A. Kugi, “Real-time nonlinear model predictive path-following control of a laboratory tower crane,” *IEEE Transactions on Control Systems Technology*, vol. 22, no. 4, pp. 1461–1473, 2013.
- [33] S. Kumar and R. Gill, “Path following for quadrotors,” in *2017 IEEE Conference on Control Technology and Applications (CCTA)*, pp. 2075–2081, IEEE, 2017.
- [34] B. Brito, B. Floor, L. Ferranti, and J. Alonso-Mora, “Model predictive contouring control for collision avoidance in unstructured dynamic environments,” *IEEE Robotics and Automation Letters*, vol. 4, no. 4, pp. 4459–4466, 2019.
- [35] D. Kloeser, T. Schoels, T. Sartor, A. Zanelli, G. Prison, and M. Diehl, “Nmpc for racing using a singularity-free path-parametric model with obstacle avoidance,” *IFAC-PapersOnLine*, vol. 53, no. 2, pp. 14324–14329, 2020.
- [36] R. Reiter, M. Kirchengast, D. Watzenig, and M. Diehl, “Mixed-integer optimization-based planning for autonomous racing with obstacles and rewards,” *IFAC-PapersOnLine*, vol. 54, no. 6, pp. 99–106, 2021.
- [37] J. Ji, X. Zhou, C. Xu, and F. Gao, “Cmpcc: Corridor-based model predictive contouring control for aggressive drone flight,” in *Experimental Robotics: The 17th International Symposium*, pp. 37–46, Springer, 2021.

- [38] A. Romero, S. Sun, P. Foehn, and D. Scaramuzza, “Model predictive contouring control for time-optimal quadrotor flight,” *IEEE Transactions on Robotics*, vol. 38, no. 6, pp. 3340–3356, 2022.
- [39] J. Arrizabalaga and M. Ryll, “Pose-following with dual quaternions,” in *2023 62nd IEEE Conference on Decision and Control (CDC)*, pp. 5959–5966, IEEE, 2023.
- [40] R. Reiter, A. Nurkanović, J. Frey, and M. Diehl, “Frenet-cartesian model representations for automotive obstacle avoidance within nonlinear mpc,” *European Journal of Control*, vol. 74, p. 100847, 2023.
- [41] T. Fork and F. Borrelli, “Euclidean and non-euclidean trajectory optimization approaches for quadrotor racing,” *arXiv preprint arXiv:2309.07262*, 2023.
- [42] M. Krinner, A. Romero, L. Bauersfeld, M. Zeilinger, A. Carron, and D. Scaramuzza, “Time-optimal flight with safety constraints and data-driven dynamics,” *arXiv preprint arXiv:2403.17551*, 2024.
- [43] P. Foehn, A. Romero, and D. Scaramuzza, “Time-optimal planning for quadrotor waypoint flight,” *Science robotics*, vol. 6, no. 56, p. eabh1221, 2021.
- [44] J. Tordesillas, B. T. Lopez, and J. P. How, “Faster: Fast and safe trajectory planner for flights in unknown environments,” in *2019 IEEE/RSJ international conference on intelligent robots and systems (IROS)*, pp. 1934–1940, IEEE, 2019.
- [45] B. Zhou, J. Pan, F. Gao, and S. Shen, “Raptor: Robust and perception-aware trajectory replanning for quadrotor fast flight,” *IEEE Transactions on Robotics*, vol. 37, no. 6, pp. 1992–2009, 2021.
- [46] H. Wang, J. Kearney, and K. Atkinson, “Arc-length parameterized spline curves for real-time simulation,” in *Proc. 5th International Conference on Curves and Surfaces*, vol. 387396, 2002.
- [47] S. Zhao, “Time derivative of rotation matrices: A tutorial,” *arXiv preprint arXiv:1609.06088*, 2016.
- [48] D. J. Struik, *Lectures on classical differential geometry*. Courier Corporation, 1961.
- [49] E. Abbena, S. Salamon, and A. Gray, *Modern differential geometry of curves and surfaces with Mathematica*. Chapman and Hall/CRC, 2017.
- [50] H. I. Choi and C. Y. Han, “Euler–rodrigues frames on spatial pythagorean-hodograph curves,” *Computer Aided Geometric Design*, vol. 19, no. 8, pp. 603–620, 2002.
- [51] Z. Šír and B. Jüttler, “ c^2 hermite interpolation by pythagorean hodograph space curves,” *Mathematics of Computation*, vol. 76, no. 259, pp. 1373–1391, 2007.
- [52] R. L. Bishop, “There is more than one way to frame a curve,” *The American Mathematical Monthly*, vol. 82, no. 3, pp. 246–251, 1975.
- [53] A. J. Hanson and H. Ma, “Parallel transport approach to curve framing,” *Indiana University, Techreports-TR425*, vol. 11, pp. 3–7, 1995.
- [54] W. Wang, B. Jüttler, D. Zheng, and Y. Liu, “Computation of rotation minimizing frames,” *ACM Transactions on Graphics (TOG)*, vol. 27, no. 1, pp. 1–18, 2008.
- [55] R. T. Farouki, *Pythagorean—Hodograph Curves*. Springer, 2008.
- [56] J. Arrizabalaga, F. Vega, Z. Šír, Z. Manchester, and M. Ryll, “Phodcos: Pythagorean hodograph-based differentiable coordinate system,” 2024.
- [57] G. Wanner and E. Hairer, *Solving ordinary differential equations II*, vol. 375. Springer Berlin Heidelberg New York, 1996.